Chapter 7

Introductory Review on an Engineering Approach for Fast-Bed Modeling in Mimic to Bubbling Bed Practice

Ming-Chuan Zhang and Chu Zhang

Additional information is available at the end of the chapter

http://dx.doi.org/10.5772/68107

Abstract

Based on the downward-penetrating particle flow through clusters and the analogy between a falling cluster and a rising bubble identified by the authors, a "type-A-choking-oriented separate-phase-coexistence model" for the upper dilute region of fast beds was established first. Without any model parameter adjustment, the unified model predicted successfully the type C choking, the solids holdup of upper dilute region, and transitions to the high-density fast bed and the dense suspension up-flow.

The model was then integrated with the sub-models of "cluster rebound at the dense bottom," "the momentum flux balances for acceleration and transition zones" in the lower and middle parts of the bed. The integrated model predicted successfully the axial solids holdup distributions of literature data under extremely wide operation conditions covering dilute-phase transportation, the premature fast bed, the classical fast bed, and the high-density fast bed.

Keywords: fast fluidization, separate-phase model, type A choking, cluster rebound, solids holdup distribution

1. Introduction

After several decades of development, fast fluidization or circulating fluidized bed (CFB) has been applied widely, nowadays, in different industries, such as chemical, metallurgy, and energy engineering [1–3]. Thanks to the particle agglomeration in CFB risers, small particles could be fluidized under quite high gas velocity, resulting in very high rates of heat and mass transfers in the bed. A unique feature of a fast fluidized bed is its nonuniform axial distribution of particle concentration. On top of the bed, the solids holdup is small, while it is large at the bottom. To form a fast fluidized bed, both of the two conditions are usually required [4]: (i) the

solid circulating rate G_s is larger than the minimum value of that G_{sm}; (ii) and at a given solid circulating rate $G_s > G_{sm}$, the superficial gas velocity u_f should be higher than the critical velocity for type C choking, but lower than that for type A choking, that is, $u_{ch,C} < u_f < u_{ch,A}$.

To predict the two-phase flow characteristics in this very special flow regime, different kinds of modeling methods have been developed. They are, for examples, two-fluid modeling based on kinetic theory established by Gidaspow [5], two-fluid modeling with energy minimization multiscale (EMMS) approach suggested by Li and Kwauk [6], CFD modeling coupled with discrete element method (DEM) [7], CFD modeling with multiphase particle-in-cell (MP-PIC) approach [8], and so on. Nowadays, these methods have been developed to an extent that three-dimensional (3D) simulation of large-scale reactors including the full-solids loop, heat and mass transfer, and reaction kinetics can be realized [9]. However, all these methods expend great amount of computer efforts, sometimes super computers are even needed [9], which is usually not affordable for engineering application.

To overcome the problems met in practice, an engineering approach for fast fluidization dynamics was proposed by the authors recently [10, 11]. This paper will give an introductory review on this approach as follows.

2. Analogy between fast beds and bubbling beds

2.1. Analogy of flows around a cluster and a bubble

To explain how a cluster is formed in a CFB riser, the wake effect was applied quite often in the literature. Recently, He et al. [12] conducted an excellent PIV investigation in a CFB riser, shown in **Figure 1(a)** and **(b)**, from which some details of this phenomenon can be seen clearly. They declared in their article, "it can be easily seen that a cluster is followed by a wake, in which particles move downward quickly," and "when a cluster is passing by, the particles are dragged down at a higher velocity." It is very clear that those particles move toward the cluster at quite high velocities, which will cause a notable deposition, yet not the one negligible, on the back side of the cluster. Considering the size limitation for a stable cluster, the same quantity of particles must be poured out from its nose. Therefore, the continuous deposition and pour out of those particles together with the downward displacement inside can be viewed as an integrated penetration of particles through the cluster. From this point of view, the phenomenon was thought quite analogous to what happens around a rising bubble in a bubbling bed, shown as in **Figure 1(c)** [13].

It can be seen that the flow patterns of the two are quite similar, except their directions being opposite-down. Moreover, the following correspondences could be easily recognized if phase-reversing is applied: (1) a rising bubble with null or few particles against a falling cluster with concentrated particles; (2) the relatively downward dense particle flow around the bubble against the upward dilute flow around the cluster; and (3) the upward-penetrating gas flow through the bubble against the downward-penetrating particle flow through the cluster. The scenarios in a CFB riser described are very close to the detailed numerical simulation results using two-fluid model combined with EMMS approach [14], that is, "the particles tend to enter

http://dx.doi.org/10.5772/68107

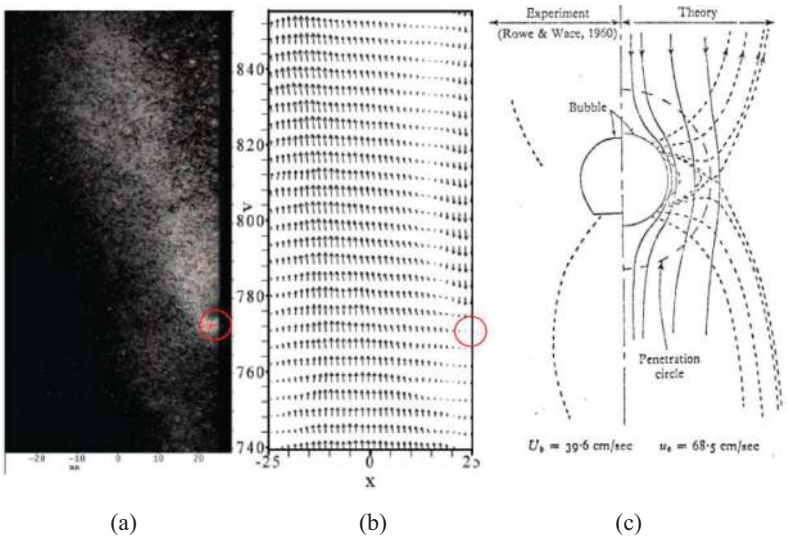

Figure 1. PIV measurement of particle moving in a CFB riser [12] compared with the flow field around a rising bubble [13]: (a) snapshots of instantaneous particle positions when a falling cluster (denoted by the small circle on the right wall) passing by; (b) corresponding particles' velocity field; and (c) flow pattern around a rising bubble.

into clusters instead of suspending in dilute broth (phase), whereas the gas tends to pass around, instead of penetrating through, the dense cluster phase" [14]. Thus, it might be possible that some results obtained from bubbling beds could be applied also to the fast fluidization, as depicted below.

2.2. Modeling strategies learned from bubbling beds

In the research progress of traditional fluidization, though people understood the phenomenon of minimum fluidization and its prediction method long time ago [15], the knowledge on fluidization had not been an applied science, to some extent, until Davidson and Harrison's bubble model appeared in 1963 [13]. This excellent model explained successfully many important phenomena of bubbling beds, and based on that, a series of reactor models of this type, that is, "bubble models," were developed [9].

What can we learn from the research success of bubbling beds? First, to grasper the critical boundary of this flow regime, that is, minimum fluidization (or minimum bubbling) in this case, is extremely important, since predicting the flow characteristics of a bubbling bed from its boundary not far away is much easier than extrapolating the flow transformation from the force analysis with a single particle. It can be seen clearly that the corresponding boundary in fast fluidization is the type A choking. And at a given gas velocity u_f, the saturation-carrying capacity or the solid flux at type A choking in a riser G_s^* corresponds to the superficial gas velocity for minimum fluidization u_{mf}. Thus, the critical boundary condition of fast fluidization, that is, the type A choking, should be studied carefully first.

Secondly, the classical two-phase theory of fluidization, that is, "above the minimum fluidization velocity, all the extra gas passes through the bed in the form of bubbles, while the rest part of the bed remains at the minimum fluidization condition" [13], is probably one form of a general law caused by the agglomeration nature of gas-solid systems. The appearing form of the general law in fast beds should be further excavated, too. It will be shown later that the formation of clusters at $G_s > G_s^*$ corresponds to the formation of bubbles at $u_f > u_{mf}$. And also, when clusters are formed, in the case of fast bed, the upward dilute flow will still be at the solid-saturated condition, as if at type A choking. All these ideas will be used for the derivation of our model below.

3. Constitutive equations for solid-saturated up-flow

3.1. Yang's formula for type A choking

To predict the happening of type A choking, much research work was carried out in the past. Among the different types of methods developed, the form of Yang's formula [16, 17] looks the one most reasonable, as the formula was derived from two simple theoretical deductions. The first one is used to calculate the terminal velocity u_t' for uniformly suspended particles with voidage ε in a riser of diameter D_t, in relative with the original value u_t for a single particle

$$u_t' = u_t \sqrt{\left(1 + \frac{f_p u_p^2}{2gD_t}\right) \times \varepsilon^{4.7}}. \tag{1}$$

where $u_p = G_s/[\rho_s(1-\varepsilon)]$ stands for the particle velocity, and f_p is the solid-wall friction factor. The formula is theoretically correct, and the detailed derivations of that can be found in the series work of Yang from 1973 to 1975 [16, 18, 19].

The second deduction is that the terminal velocity of a particle suspension in a finite diameter riser u_t', that is, the slip velocity between gas and solid, is just equal to the terminal velocity of a single particle in the infinity u_t, when type A choking occurs [16, 17]

$$u_t' = u_t. \tag{2}$$

In the derivation of Yang's predictive equation (Eq. (3)), this deduction was actually applied [16, 17], yet not declared clearly

$$\frac{2D_t g(\varepsilon_{ch}^{-4.7} - 1)}{(u_{ch} - u_t)^2} = f_p. \tag{3}$$

The original value of solid-wall friction factor f_p was taken as 0.01 in 1975 [16], but it was changed in 1983 to the present form as [17]

$$f_p = 6.81 \times 10^5 \left(\frac{\rho_g}{\rho_s}\right)^{2.2}. \tag{4}$$

http://dx.doi.org/10.5772/68107

3.2. Physical essence of Yang's formula

From Eq. (1), it can be easily recognized that the influence of wall friction on u'_t is reflected by the first item with square root sign $\sqrt{[1+f_p u_p^2/(2gD_t)]}$, since for an infinitely wide riser it will always be unity. With a decrease of D_t, the wall friction increases, then u_t' increases. And the influence of bed voidage, that is, the influence of surrounding particles, is reflected by the second item with square root sign $\sqrt{\varepsilon^{4.7}}$. With an increase of particle concentration (1–ε), ε decreases, and then u_t' decreases. This is because when the concentration of particles increases, the real gas velocity ($1/\sqrt{\varepsilon^2}$) increases, and the flow path of gas around the particle considered becomes more flexuous, and then the drag force coefficient will increase ($1/\sqrt{\varepsilon^{2.7}}$), too [14].

To quantitatively analyze further the overall force balance for a uniform suspension of particles in a gas flow, we can resolve the increased fluid drag into the basal fluid drag on a single particle F_f and the surplus F_s due to the surrounding particles. Then, we have

$$F_f + F_s = G + W, \tag{5}$$

where G is the gravity of particle suspension, while W stands for the friction of riser wall.

If we compare the values of F_s and W, we will have two different situations. When the suspension is quite dilute, the surplus drag force is relatively small. Then, we will have $F_s < W$, and $F_f > G$. The latter means that subtracting particle gravity the basal fluid drag F_f still have something rest with its own freedom, resulting in $F_f - G = W - F_s$ and a simple dynamic system centered on each single particle. That is the case of normal dilute transportation, because the relatively independent movement of these particles will let themselves disperse uniformly. On the other hand, if we have $F_s > W$ and $F_f < G$, the basal fluid drag F_f will no longer be able, by itself, to support the particle but requires help from surrounding particles, as $F_f + (F_s - W) = G$. That makes the dynamic system more complex and easier to lose its uniformity, since the force balance of any single particle depends more on the others.

Therefore, the criteria of $F_s = W$ or $F_f = G$ can be used to separate the two different situations just mentioned. Clearly, this critical condition is the type A choking, where the influence of bed voidage on u_t' is just compensated by the influence of riser wall, leading to $u_t' = u_t$. At this unique condition, a moving particle looks as if there is neither surrounding particles nor the riser wall. From the authors' opinion, this is the real physical essence of type A choking. Then, the functional dependence of the bed voidage on the superficial gas velocity at type A choking, that is, Eq. (3), could be used as the "constitutive equation" for solid-saturated up-flow.

3.3. Reconstruction of Yang's formula

According to a comprehensive review paper on choking for vertical conveying systems by Xu et al. [20], the prediction accuracy of Yang's formula is not satisfactory for type A choking, though it was suggested to be applied for a pretty long time [21]. In conserving its form, the solid-wall friction factor f_p in Yang's formula was recorrelated by the authors [10] with the data collected by Xu et al. [20], resulting in

$$f_p = 0.01\left(\frac{u_f - u_t}{u_t}\right)^{\alpha}\left(\frac{gD_t}{0.8u_t^2}\right)^{\vartheta} \tag{6}$$

$$\alpha = -(1.0723 + 0.0017\mathrm{Ar}). \tag{7}$$

When $gD_t/u_t^2 > 0.8$, $\vartheta = 0.71$; while $gD_t/u_t^2 < 0.8$, $\vartheta = -1.27$, as shown in **Figure 2**. This correlation is applied with Ar = 1–1000, $u_{ch,A}/u_t$= 3–40, and gD_t/u_t^2 = 0.2–1000. And the values of f_p should range from 0.001 to 0.1. As can be seen in **Figure 3**, the predicted saturation-carrying capacities G_s^* are in good consistency with the experimental data, if some observation delays in these experiments are considered.

The dependence of dimensionless solid-wall friction factor $\tilde{f}_p$ on dimensionless riser diameter gD_t/u_t^2 changes abruptly at $gD_t/u_t^2 = 0.8$, which corresponds to the transit of general flow pattern from confined slugging to free bubbling [10]. It further confirms that type A choking is a riser-diameter-dependent phenomenon, as we discussed before. However, most of the previous work ignored this dependence except Xu et al. [20], showing that the influence of

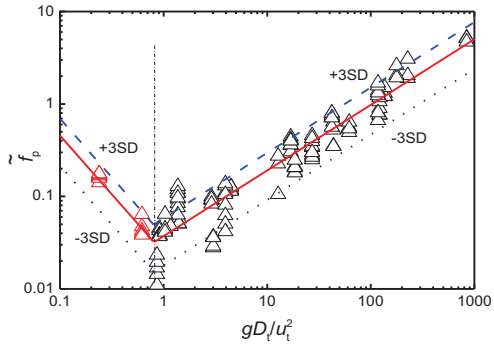

Figure 2. Log-log plot of $\tilde{f}_p$ with gD_t/u_t^2 for experimental data collected by Xu et al. [20].

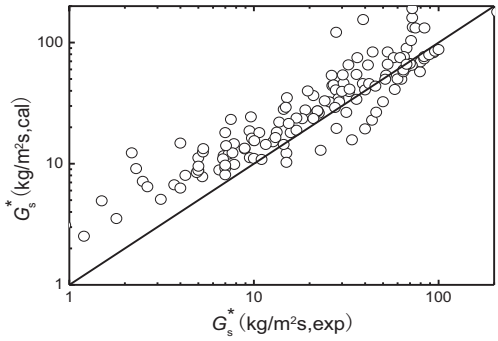

Figure 3. Predictions of G_s^* for type A choking compared with experimental data of [20].

http://dx.doi.org/10.5772/68107

riser diameter on type A choking velocity was not monotonic. Since the new correlation is given in a dimensionless form and the application ranges are quite wide, it is hoped that this correlation could be used, to some extent, in practically large units. For instance, if the particle terminal velocity is around 0.3 m/s (typical in CFB boilers), the riser diameter could be used up to 10 m.

4. Separate-phase-coexistence model for fast bed

4.1. Physical description of the model

Described above, Eq. (3) gives the functional dependence of bed voidage ε_{ch} on superficial gas velocity u_{ch} under solid-saturated conditions. For a given fluidizing system, with an increase of u_{ch}, ε_{ch} decreases and $(1-\varepsilon_{ch})$ increases, and then the solid flux at type A choking G_s^* will increase more rapidly

$$G_s^* = \rho_s(u_{ch} - u_t)\frac{1-\varepsilon_{ch}}{\varepsilon_{ch}}. \tag{8}$$

Taking an FCC-air fluidizing system as an example, **Figure 4** shows the calculated $(1-\varepsilon_{ch})$ and G_s^* varied with u_f. Thanks to this special dependence of G_s^* on u_f (u_{ch} in the equation), the system will not completely collapse when the circulating solid flux is greater than G_s^* corresponded to the superficial gas velocity u_f. Some particles will segregate from the gas stream to form a free-sedimentary dense phase, that is, the so-called cluster. The fluidizing system then runs in a more complicated separate-phase-coexistence mode. The cluster occupies a part of the cross-sectional area of the riser, but without any outer gas invading in. Meanwhile in the rest part of the riser, all gas squeezes into the dilute phase and carries much more particles upward.

Let β stand for the fraction of cross-sectional area occupied by the falling clusters, and m_s^- for the solid flux downward, while m_s^+ represent the solid flux upward in the dilute phase. Both

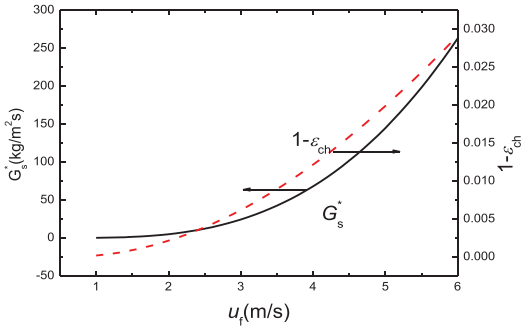

Figure 4. Dependences of solid flux G_s^* and its concentration $(1-\varepsilon_{ch})$ at type A choking on superficial gas velocity u_f for an FCC-air system (ρ_s= 1620 kg/m^3, d_p= 100 μm, D_t= 0.1 m).

m_s^+ and m_s^- are calculated based on the total cross-sectional area of the riser, but not their own occupied. Then, the circulating solid flux in the riser G_s should be

$$G_s = m_s^+ - m_s^-. \tag{9}$$

Figure 5 shows the schematic diagram of m_s^+ and m_s^- calculated for varied β at a given gas velocity.

This figure shows when

$$\left.\frac{dm_s^+}{d\beta}\right|_{\beta=0} > \left.\frac{dm_s^-}{d\beta}\right|_{\beta=0}, \tag{10}$$

more particles, compared with those at type A choking, can be transported upward in the separate-phase-coexistence mode, that is, $G_s = m_s^+ - m_s^- > G_s^*$. However, when β increases to a critical value β_{ch}

$$\left.\frac{dm_s^+}{d\beta}\right|_{\beta=\beta_{ch}} = \left.\frac{dm_s^-}{d\beta}\right|_{\beta=\beta_{ch}}, \tag{11}$$

the net solid flux transported upward reaches its maximum value $G_{s,max}$. Beyond that point, the system will be abruptly collapsed, that is, the case of type C choking.

Therefore, the basal requirement for separate-phase-coexistence mode should be

$$\left.\frac{dm_s^+}{d\beta}\right|_{\beta=0} >= \left.\frac{dm_s^-}{d\beta}\right|_{\beta=0}. \tag{12}$$

This criterion will be applied later to predict G_{sm}, the minimum solid flux for fast bed.

"Without outer-gas invaded in clusters" is a primary assumption used in our model. Its necessary condition is met by the downward penetration of solid particles into the cluster, in

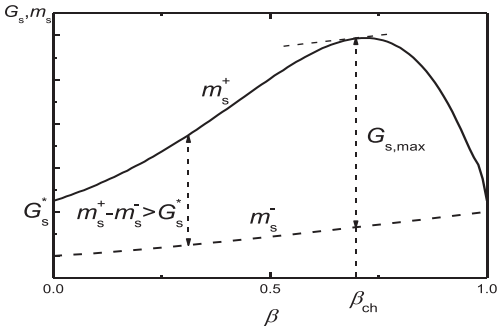

Figure 5. Schematic diagram of m_s^+ and m_s^- changed with β at given gas velocity.

http://dx.doi.org/10.5772/68107

which there is always an upward interstitial gas flow subject to the pressure gradient of the bed. There have not been direct experimental evidences for the sufficient condition, that is, the two opposite flows should be completely compensated with each other. However, it is speculated that this situation could be the one with least flow resistance for a gas-solid two-phase system with agglomerative nature, and then tends to be most possible. In analogy with the bubbling beds, "no outer-gas invading clusters" is surely corresponding to "no solid particles falling into bubbles."

4.2. Mathematical model kernels

4.2.1. Model kernels

At the very beginning of cluster formation ($\beta \approx 0$), the terminal velocity of a single particle u_t can still be used as the gas-solid slip velocity, the same value at type A choking. It is surely expected, when clusters visibly appear, the gas-solid slip velocity will increase due to the impact of falling clusters. To facilitate the calculation, this impact can be realized with decreasing the effective gas velocity of dilute phase by an effective velocity factor of $F(\beta) < 1$. Therefore, the upward solid flux based on unit dilute-phase area should be

$$G_s^+ = \rho_s \left[\frac{u_f F(\beta)}{1-\beta} - u_t \right] \frac{1-\varepsilon_{ch}}{\varepsilon_{ch}}. \tag{13}$$

Meanwhile, the solid-saturated dilute-phase voidage ε_{ch} and the nominal gas velocity $u_{ch}^* = u_f F(\beta)/(1–\beta)$ should still fit the revised Yang's formula. Then, the kernel model for dilute phase, that is, the superficial upward solid flux based on unit cross-sectional area of the riser, is expressed as

$$m_s^+ = \rho_s [u_f F(\beta) - u_t(1-\beta)] \frac{1-\varepsilon_{ch}}{\varepsilon_{ch}}. \tag{14}$$

The form of the kernel model for dense phase or falling clusters is quite simple as

$$m_s^- = \rho_s \beta u_{cl}(1-\varepsilon_{cl}). \tag{15}$$

Meanwhile, to keep the outer-gas flow within the cluster being zero, the modified Richardson-Zaki's equation [22] must be satisfied for the cluster voidage ε_{cl} and its falling velocity u_{cl}. Then, we have

$$u_{cl} = u_t \left(\frac{\varepsilon_{cl}}{1} \right)^m = u_t \varepsilon_{cl}^m. \tag{16}$$

Here,

$$m = \lg\left(\frac{u_{mf}}{u_t} \right) \Big/ \lg \varepsilon_{mf}, \tag{17}$$

and the value of voidage at minimum fluidization $\varepsilon_{mf} = 0.45$ was taken in later calculations.

4.2.2. Empirical closures for F(β) and ε_{cl}

To make the kernel model for dilute phase closed, an empirical expression for the effective velocity factor $F(\beta)$ was given as [10]

$$F(\beta) = 1 - [1 - F(1)]\beta^n, \tag{18}$$

where $F(1)$ is the value of $F(\beta)$ at β=1 and can be calculated as

$$F(1) = \left(1 - \frac{u_t}{u_f}\right)\frac{1 - \varepsilon_{ch,A}}{\varepsilon_{ch,A}}\frac{\varepsilon_{sl}}{1 - \varepsilon_{sl}}, \tag{19}$$

ε_{sl} and $\varepsilon_{ch,A}$ are the bed voidages for slugging (β=1) and type A choking (β=0), respectively.

Here,

$$\varepsilon_{sl} = 1 - (1 - \varepsilon_{mf})/2. \tag{20}$$

To make the kernel model for dense phase closed, Harris's correlation [23] for solid concentration in clusters $\varepsilon_{s,\,cl}$ was suggested be applied [11].

$$1 - \varepsilon_{cl} = \varepsilon_{s,cl} = \frac{0.58(\varepsilon_s^*)^{1.48}}{0.013 + (\varepsilon_s^*)^{1.48}}, \tag{21}$$

where ε_s^* is the solids holdup in upper dilute region, which will be discussed in Section 4.4. Or, an even rough estimation directly from ε_{ch} could be used as

$$1 - \varepsilon_{cl} = 2(1 - \varepsilon_{ch}) + 0.45\beta. \tag{22}$$

With these equations derived, the calculation procedure is quite straightforward. (i) Type A choking velocity $u_{ch,A}$ is calculated for a given solid flux $G_s > G_{sm}$. (ii) Decreasing superficial gas velocity to make $u_f < u_{ch,A}$; then, m_s^+ and m_s^- are calculated by using different β until $G_s = m_s^+ - m_s^-$ is satisfied; the voidage of upward dilute phase ε_{ch} at the operating gas velocity u_f is then determined. (iii) Repeating the steps above until type C choking occurs, the type C choking velocity $u_{ch,C}$ is finally obtained.

Using different model parameter n, the variations of dilute-phase voidage ε_{ch} with operating gas velocity u_f for an FCC-air system are shown in **Figure 6**. It can be seen from the figure that when the operating gas velocity u_f is close to $u_{ch,C}$, a small reduction of gas velocity will cause a great increase of solid concentration ($1-\varepsilon$) and then pressure drop of the bed. Thus, it can be recognized as the occurrence of type C choking.

The figure also shows that the type C choking velocity calculated decreases with an increase of n used. Since Yousfi and Gau's empirical correlation for type C choking [24] (Eq. (23)) had been considered as the best in the literature [20], it was applied to estimate the proper value of n

$$\frac{u_{ch,C}}{\sqrt{gd_p}} = 32\mathrm{Re}_t^{-0.06}\left(\frac{G_s}{\rho_g u_{ch,C}}\right)^{0.28}. \tag{23}$$

http://dx.doi.org/10.5772/68107

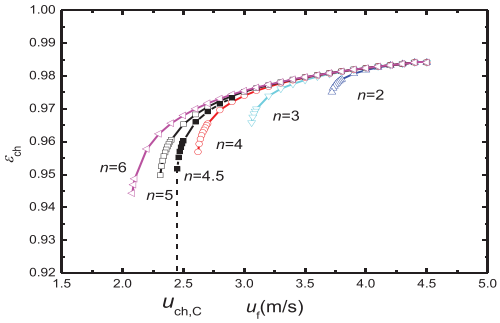

Figure 6. Variations of dilute-phase voidage ε_{ch} with gas velocity u_f calculated from different n for an FCC-air system (D_t= 0.1 m, ρ_s= 1620 kg/m^3, d_p= 100 μm, G_s= 100 kg/(m^{2}s)).

From this kind of "calibration," the model parameter $n = 4.5$ was chosen for a simplified version of the model without iteration. **Figure 7** shows comparisons between the model predicted $u_{ch,C}$ with $n = 4.5$ and those given by Eq. (23), for both FCC-air and sand-air systems with different particle sizes (50, 100, 150, and 200 μm) and solid fluxes (50, 100 and 200 kg/(m^{2}s)) in a riser of 0.1 m, typical scale in laboratories. The result looks quite satisfactory.

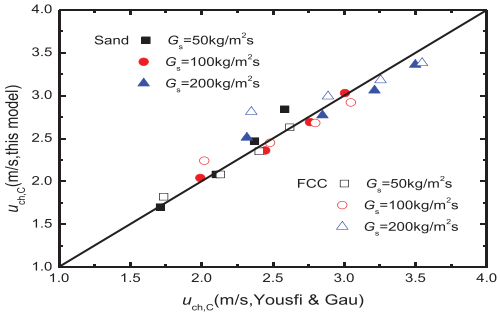

Figure 7. Comparison of model predictions for type C choking ($n = 4.5$, D_t= 0.1 m) and those from Yousfi and Gau [24].

4.2.3. Mechanistic closures for F(β) and ε_{cl}

From a meso-scale analysis in mimic to bubbling beds [10], the effective velocity factor in dilute phase $F(\beta)$ was determined as

$$F(\beta) = 1 - \frac{3u_{pen}}{u_f} \cdot \frac{1-\varepsilon_{cl}}{\varepsilon_{cl}} \cdot \frac{\varepsilon_{ch}}{1-\varepsilon_{ch}} \cdot \beta \cdot \varphi, \tag{24}$$

where u_{pen} stands for the superficial percolation velocity in a packed bed of voidage ε_{cl} under pressure gradient of the bed, and φ is the influence factor of penetrating particles in clouds

$$\varphi = \left(\frac{u_{cl} + 2u_{sd,\infty}}{u_{cl} - u_{sd,\infty}} - 1\right) \frac{\beta}{1-\beta}. \tag{25}$$

Detailed definitions and calculation methods of these parameters in Eqs. (24) and (25) can be found in Ref. [10].

It will be discussed later in Section 5.1, the weight of clusters should be balanced by the inter-phase drag between the dilute and the dense phases. This requirement can be used to determine the cluster voidage ε_{cl} independently, rather than using Harris's correlation. Certainly, all these calculations need iterations.

As an example, **Figure 8** shows that the meso-scale model determined $F(\beta)$ compared with those with constant n for an FCC-air system. It can be seen that $n = 4.5$ is a pretty good approximation for the simplified version without iterations. And **Figure 9** shows the solid concentration of clusters predicted by inter-phase balance compared with Harris's correlation. It can be seen that they are also in agreement with each other pretty well.

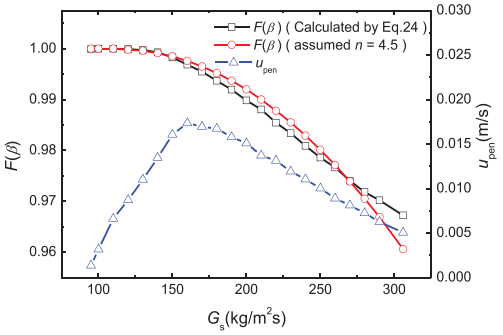

Figure 8. F(β) calculated by Eq. (24) compared with constant n (FCC-air system, $\rho_s = 1600$ kg/m^3, $d_p = 70$ μm, $D_t = 0.1$ m, $u_f = 6$ m/s).

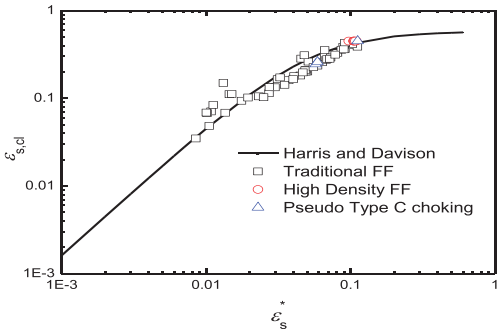

Figure 9. Predicted solid concentration of clusters $\varepsilon_{s,cl}$ compared with Harris's correlation [23].

As a first check, **Figure 10** shows the solid flux G_s^C at type C choking predicted by the mechanistic model. The model predictions were compared with the experimental data collected by Xu et al. [20]. Noting that some data points of type B choking due to blower and/or standpipe limitation of the system [21] could also be included, the accuracy of model prediction is reasonably accepted.

http://dx.doi.org/10.5772/68107

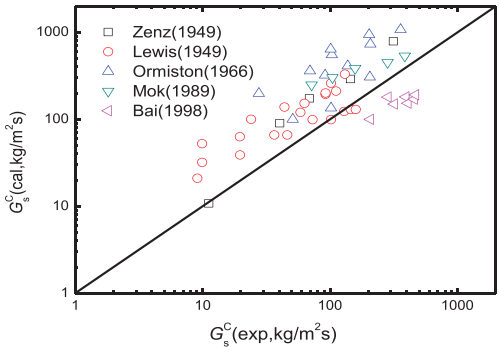

Figure 10. Predictions of $G_s{}^C$ for type C choking compared with the experimental data collected by Xu et al. [20].

4.3. Minimum solid flux for fast bed

As mentioned before, the critical requirement for separate-phase-coexistence mode is

$$\left.\frac{\mathrm{d}m_s^+}{\mathrm{d}\beta}\right|_{\beta=0} = \left.\frac{\mathrm{d}m_s^-}{\mathrm{d}\beta}\right|_{\beta=0}, \tag{12a}$$

which can be used for the determination of G_{sm}, the minimum solid flux for fast bed. And we have already

$$m_s^+ = \rho_s[u_f F(\beta) - u_t(1-\beta)]\frac{1-\varepsilon_{ch}}{\varepsilon_{ch}} \tag{14a}$$

$$m_s^- = \rho_s \beta u_{cl}(1-\varepsilon_{cl}). \tag{15a}$$

The derivation of Eq. (15a) is quite straightforward, that is,

$$\left.\frac{\mathrm{d}m_s^-}{\mathrm{d}\beta}\right|_{\beta\to 0} = \rho_s u_{cl}|_{\beta\to 0}(1-\varepsilon_{cl})|_{\beta\to 0}. \tag{26}$$

And, as we have also [11]

$$(1-\varepsilon_{cl})|_{\beta\to 0} = 2(1-\varepsilon_{ch,A}) \tag{27}$$

$$u_{cl}|_{\beta\to 0} = u_t \times (\varepsilon_{cl}|_{\beta\to 0})^m = u_t[1-2(1-\varepsilon_{ch,A})]^m \approx u_t. \tag{28}$$

The first statement means that at the very beginning of phase separation, the original formation of cluster is due to a noncollided convergence of two dilute solid pockets. The second statement with equal signs is required for the force balance of gas and particles inside the clusters settled freely, that is, the modified Richardson-Zaki equation should be fitted [11]. Because the solid concentration of the originally formed cluster is very small, the voidage is

close to unity, its falling velocity can then be estimated as the particle terminal velocity u_t. Putting Eqs. (27) and (28) into Eq. (26), we have approximately

$$\frac{\mathrm{d}m_s^-}{\mathrm{d}\beta}|_{\beta\to 0} \approx 2\rho_s u_t(1-\varepsilon_{ch,A}). \tag{29}$$

To obtain the derivative of m_s^+ with respect to β directly is difficult, since both $F(\beta)$ and ε_{ch} in Eq. (14a) change with β in very complicated manners. However, the expression for m_s^+ can be linearized, under conditions of very small β ($\beta \approx 0$) as

$$m_s^+|_{\beta\approx 0} = (1+k\beta)G_s^*. \tag{30}$$

Here, k stands for an unknown coefficient to be determined numerically later. Then, the derivative can be written as

$$\left.\frac{\mathrm{d}m_s^+}{\mathrm{d}\beta}\right|_{\beta\approx 0} = kG_s^* \quad = k\rho_s(u_{ch,A}-u_t)\frac{1-\varepsilon_{ch,A}}{\varepsilon_{ch,A}} \approx k\rho_s(u_{ch,A}-u_t)(1-\varepsilon_{ch,A}) \tag{31}$$

Let the terms on the right side of Eqs. (29) and (31) be equal, we have

$$k^*\rho_s(u_{ch,A}^*-u_t) \approx 2\rho_s u_t. \tag{32}$$

Here, $u_{ch,A}^*$ and k^* are $u_{ch,A}$ and k evaluated at the minimum solid flux G_{sm}, respectively. Therefore, we obtain

$$u_{ch,A}^* \approx \left(\frac{2}{k^*}+1\right)u_t. \tag{33}$$

The values of k can be calculated numerically for different small values of β, according to the definition of $k = (m_s^+/G_s^+ - 1)/\beta$. Taking 60-μm FCC particles fluidized in a 0.1−m diameter riser as an example, the results obtained are shown in **Figure 11**. From reasonable extrapolation,

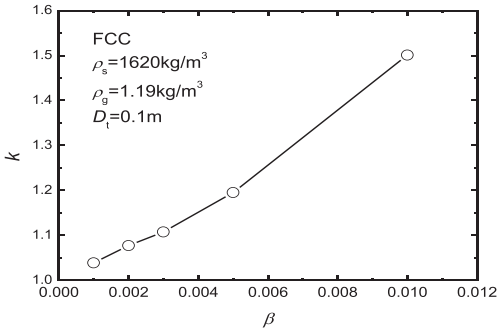

Figure 11. Variation of coefficient k in Eq. (30) with β for 60-μm FCC particles in a 0.1-m diameter riser.

http://dx.doi.org/10.5772/68107

it can be concluded that the coefficient k under the condition of $\beta \to 0$ is approximately one, that is, $k^* \approx 1$. Finally, we have a very simple result, that is,

$$u^*_{ch,A} \approx 3u_t. \tag{34}$$

Correspondingly, the minimum solid flux G_{sm} for fast fluidization can be estimated by the revised Yang's formula at superficial gas velocity of $3u_t$.

Figure 12 shows comparison between the values of G_{sm} determined from $3u_t$ and those from $u_{ch,C}$ and $u_{ch,A}$ becoming equal, for 60-μm FCC particles in a 0.1−m diameter riser. It can be seen from the figure that the comparison is quite satisfactory.

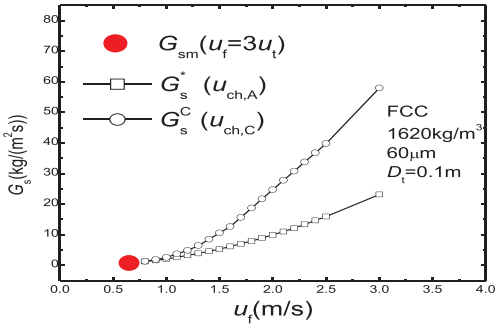

Figure 12. G_{sm} determined from $3u_t$ compared with $u_{ch,C}$ and $u_{ch,A}$ becoming equal, for 60-μm FCC particles in a 0.1-m diameter riser.

The minimum solid flux for fast bed is generally more important in theory than in practice, since in most practical circulating fluidized bed systems the solid flux is usually much higher than G_{sm}. However, there might be a potential practical application for circulating fluidized bed combustion of coal, where particle size distribution is quite wide, but the gas velocity is relatively low. Therefore, it is possible that the gas velocity is higher than the minimum value required for fast fluidization with respect to the average particle size $3u_{t(dp,ave)}$, but not high enough for some coarse particle fractions. In this case, the value of $u_{t(dp,crit)} = u_f/3$ may be used as a criterion, by which the whole particle size distribution can be divided into two relatively narrow groups, $d_p \le d_{p,crit}$ and $d_p > d_{p,crit}$. It is suggested that only the finer particle group with its own average size be calculated with the model, while the coarse particle group be treated as a stationary fluidized bed.

4.4. Solids holdup in upper dilute region

As we mentioned earlier, Eq. (1) was proposed by Yang to amend the terminal velocity of a uniform particle suspension in a CFB riser u'_t [16, 17]. The influence of wall friction on u_t' appears in the form of $\sqrt{[1+f_p u_p{}^2/(2gD_t)]}$. In a finite diameter riser, besides the particle gravity the gas drag at u_t' will also conquer the wall friction. Considering the influence of wall friction as additional particle gravity, the equivalent gravity factor is determined as

$$k_w = \left(1 + \frac{f_p u_p^2}{2gD_t}\right). \tag{35}$$

The concept of k_w can also be applied to the case of separate-phase-coexistence if the falling clusters are considered as a moving wall, in which the dilute-phase flows upward. In this case, the slipping velocity of those particles relative to the "cluster wall" will increase from u_p to

$$u_p^{'} = u_p + \beta u_{cl} = \frac{G_s^+}{\rho_s(1-\varepsilon_{ch})} + \beta u_{cl}. \tag{36}$$

Meanwhile, the equivalent diameter of the flow path will decrease from D_t to D_t', which is determined as [10, 11]

$$\frac{1}{D_t^{'}} = \frac{1}{D_{t1}} + \beta\left(\frac{1}{D_{t2}} - \frac{1}{D_{t1}}\right), \tag{37}$$

where D_{t1} is the equivalent flow-path diameter for very small cluster fraction β, while clusters tend to move close to the wall

$$D_{t1} = D_t\sqrt{1-\beta}. \tag{38}$$

And D_{t2} is the equivalent flow-path diameter for very big cluster fraction β, while clusters have to distribute uniformly in the riser

$$D_{t2} = \frac{4F}{U} = D_t\frac{1-\beta}{1+1.5\beta\frac{D_t}{D_{cl}}}, \tag{39}$$

where F and U are the cross-sectional area and the wetted perimeter of the "tubing" dilute flow, respectively, while Dcl is the diameter of cluster, which can be estimated from the empirical correlation given by Harris and Davidson (Eq. (40)) [23] or the dimensionless form suggested by the authors (Eq. (41)) [10] (see also **Figure 13**).

$$D_{cl} = \frac{1-\overline{\varepsilon}}{40.8 - 94.5(1-\overline{\varepsilon})}\,[\mathrm{m}] \tag{40}$$

$$\frac{D_{cl}}{D_t} = 27.34(1-\overline{\varepsilon})^{1.26}\left(\frac{gD_t}{2u_t^2} + 1.5\right)^{-1}, \tag{41}$$

where ε^- is the average voidage of the upper dilute region.

The reason that we could treat the meso-scale drag using the concept of equivalent wall friction with viscous drag only, same as the riser wall, is due to the suppression effect of penetrating particles on the wake separation behind the cluster, which is discussed in detail in Ref. [11].

By using the concept of equivalent gravity, the pressure gradient in the upper dilute region can be expressed as [10]

http://dx.doi.org/10.5772/68107

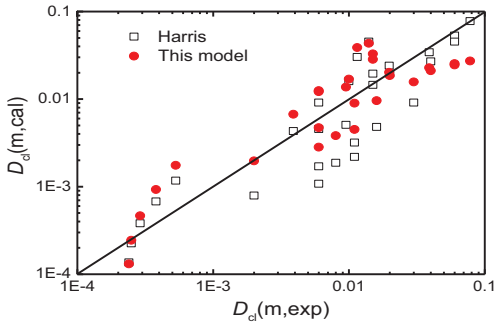

Figure 13. Cluster size predictions from different correlations compared with experimental data collected by Harris et al. [23].

$$-\frac{dp}{dz} = (1-\varepsilon_{ch})\rho_s g\left(1+\frac{f_p u_p'^2}{2gD_t'}\right)(1-\beta), \tag{42}$$

where ε_{ch} is the dilute-phase voidage calculated by this model. In the equation, $(1-\varepsilon_{ch})\rho_s g$ is the particle weight in dilute phase, $(1-\varepsilon_{ch})\rho_s g \times f_p u_p'^2/(2gD_t')$ is the equivalent "wall" friction, while $(1-\beta)$ represents the time fraction when the upward dilute phase is sensed by the pressure probe.

From the analysis above, the apparent solids holdup in the upper dilute region can be easily predicted as

$$\varepsilon_s^* = -\frac{dp}{dz}/(\rho_s g) = \varepsilon_{s,ch}\left(1+\frac{f_p u_p'^2}{2gD_t'}\right)(1-\beta). \tag{43}$$

Here, $\varepsilon_{s,ch} = (1-\varepsilon_{ch})$ is the solid concentration in upward dilute phase. Since the calculation of D_{cl} (Eqs. (40) or (41)) involves $(1-\bar{\varepsilon}) = \varepsilon_s^*$, iterations should be applied. The initial value of $(1-\bar{\varepsilon})$ for iteration is suggested as $(1-\bar{\varepsilon})_0 = \varepsilon_{s,ch}+0.25\beta$.

There were quite a lot of theoretical and experimental investigations on the solids holdup of the upper dilute region in the literature. Among them, Ouyang and Potter compiled abundant data available at that time [25], where the solids holdups of the upper dilute regions and the corresponding operating conditions were both reported in detail. Using the operating conditions provided, the solids holdups of the upper dilute regions were calculated with the model and compared with the experimental data in **Figure 14**. In the figure, symbols of 1–4 indicate the conditions of dilute transportation, traditional fast fluidization, high-density fast fluidization (HDFF) (to be discussed later in Section 5), and pseudo type C choking, respectively. The figure shows that the predictions for traditional fast fluidization, high-density fast fluidization, and pseudo type C choking are reasonably good. However, predicted ε_s^* for dilute transportation (denoted as hollow squares in the figure) are all lower than those from experiments. The reason for under-prediction of ε_s^* in those cases might be under-evaluation of the terminal velocity u_t. It would often be met for particles with certain size distribution.

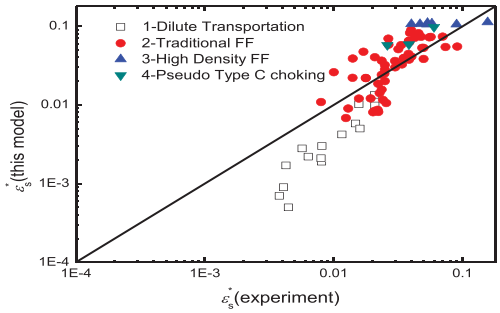

Figure 14. Predictions of solids holdup for the upper dilute region ε_s^* compared with experimental data collected by Ouyang and Potter [25].

5. Transition to high-density fast bed

5.1. Force balance of falling clusters

As discussed above, besides its gravity the upward dilute phase should also conquer the equivalent "wall" friction F_w in a fast-bed riser [10]

$$F_w = (1-\varepsilon_{ch})\rho_s g \frac{f_p u_p'^2}{2gD_t'}. \tag{44}$$

The equivalent friction is caused by both falling clusters and the riser wall. The latter can be estimated from the wall friction at the type A choking F_{w0}, since falling clusters have not yet formed at that moment

$$F_{w0} = (1-\varepsilon_{ch,A})\rho_s g \frac{f_p u_p^2}{2gD_t}. \tag{45}$$

Then, the net inter-phase drag between the upward dilute phase and falling clusters can be estimated as

$$\Delta F_w = F_w - F_{w0}. \tag{46}$$

On the other hand, the gravity of falling clusters is easily calculated as

$$G_{cl} = \beta(1-\varepsilon_{cl})\rho_s g. \tag{47}$$

As we mentioned above in Section 4.2.3 (closure to dense phase model), the weight of clusters should always be balanced with the inter-phase drag. By using the initial value of $\varepsilon_{cl,0}$ (Eq. (22)), the inter-phase drag ΔF_w calculated is usually not just equal to the cluster gravity G_{cl}. Then, sequence adjustments for u_{cl} and/or ε_{cl} will be done with iterations until a new balance of $\Delta F_w = G_{cl}$ is reached. At a relatively low-operating velocity of gas, the adjustment of u_{cl} and ε_{cl} is reciprocally supported. With an increase of G_s, the cluster-falling velocity u_{cl} and

its voidage ε_{cl} decrease simultaneously, until type C choking happens. This is the case of traditional fast fluidization, where clusters settle down freely as we discussed above.

5.2. Secondary fluidization of clusters

On the other hand, if the operating velocity of gas is high enough, the situation could be different. When G_s increases to a certain value of G_s^{**}, the cluster voidage ε_{cl} reaches its minimum value $\varepsilon_{cl,min}$, the minimum voidage of clusters. In the case of $G_s > G_s^{**}$, the adjustments of u_{cl} and ε_{cl} are no longer reciprocally supported, since the voidage of clusters is fixed to $\varepsilon_{cl,min}$. Therefore, the adjustment for $\Delta F_w = G_{cl}$ can be performed by reducing the cluster-falling velocity along. Compared with its original value, that is, the one determined by the modified Richardson-Zaki's equation for the voidage $\varepsilon_{cl} = \varepsilon_{cl,min}$, the minus adjustment for falling velocity of clusters can be signed as (-)u^*. To keep the relative velocity of gas and particles inside the cluster unchanged, a small quantity of outer gas has to invade into the cluster at the same velocity u^*. As a result, the cluster gets a tendency of moving upward, but no longer be free settling. This phenomenon might be termed as "secondary fluidization of clusters" (SFC), somewhat similar to the fluidization of packed particles.

Detailed model modifications for $G_s > G_s^{**}$ can be found in Ref. [10], in which the most important ones are listed below:

$$m_s^{+} = \rho_s[(u_f - \beta u^*)G(\beta) - u_t(1-\beta)]\frac{1-\varepsilon_{ch}}{\varepsilon_{ch}} \tag{48}$$

$$m_s^{-} = \rho_s \beta (u_{cl} - u^*)(1-\varepsilon_{cl}). \tag{49}$$

Here, $G(\beta)$ stands for the modified effective velocity factor of dilute phase for $G_s > G_s^{**}$

$$G(\beta) = 1 - \frac{3(u_{pen} - u^*)}{u_f} \cdot \frac{1-\varepsilon_{cl}}{\varepsilon_{cl}} \cdot \frac{\varepsilon_{ch}}{1-\varepsilon_{ch}} \cdot \beta \cdot \varphi \text{ for } 0 < u^* < u_{pen}, \tag{50}$$

$$G(\beta) = \frac{u_f - \beta u_{pen}}{u_f - \beta u^*} \text{ for } u^* > u_{pen}. \tag{51}$$

5.3. Prediction to transition of HDFF

The model predictions to Issangya's experiment [26] for $u_f = 6$ m/s are shown in **Figure 15(a)**. It can be seen from the figure that the model properly predicted the unique feature of high-density fast fluidization, that is, the solids holdups of the upper dilute region and the bottom-dense region do not change obviously with further increase of $G_s > G_s^{**}$. And **Figure 15(b)** shows that the final falling velocity of clusters $u_{cl}^* = u_{cl} - u^*$ (opposite direction of u_f as positive) decreases continuously with an increase of G_s. When $u^* > u_{cl}$, u_{cl}^* becomes negative, this means all the clusters will move upward. This is the flow regime defined by Grace et al. as "dense suspension up-flow" (DSU) [27].

According to Issangya's experiment [26], the solid-gas mass ratio at the onset of high-density fast fluidization was about 40. And Grace et al. proposed a more general correlation for the onset of dense suspension up-flow as [27]

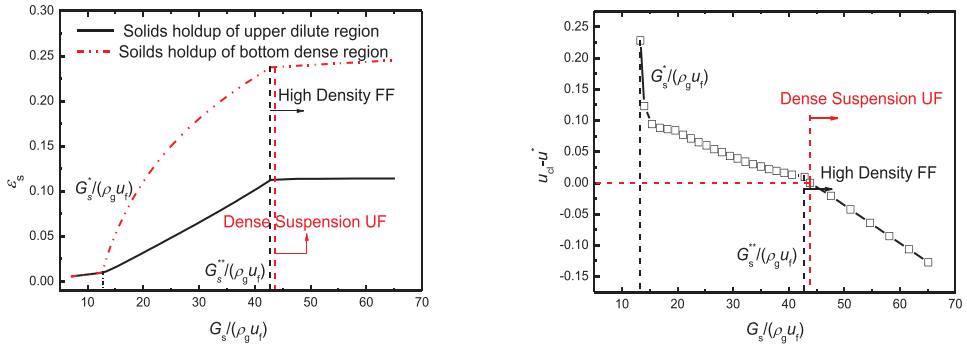

Figure 15. Transition from traditional fast bed to HDFF for an FCC-air system ($\rho_s = 1600$ kg/m^3, $d_p = 70$ μm, $D_t = 0.076$ m, $u_f = 6$ m/s): (a) solids holdups of upper dilute region and bottom-dense region; (b) falling velocity of clusters.

$$U_{DSU} = 0.0113 G_s^{1.192} \rho_g{}^{-1.064} [\mu_g g(\rho_s - \rho_g)]^{-0.064}. \quad (52)$$

The model predictions to the onsets of high-density fast bed and dense suspension up-flow for FCC and sand particles fluidized by ambient air are compared with those given by Issangya et al. [26] and Grace et al. [27] in **Figure 16**, respectively. The results are also reasonably good.

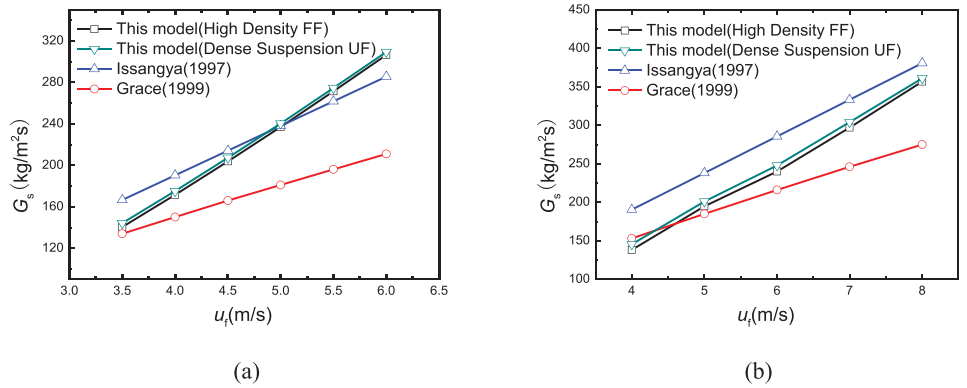

Figure 16. Comparisons of onsets of HDFF and DSU predicted from different models or criteria: (a) FCC-air, $\rho_s = 1600$ kg/m^3, $d_p = 70$ μm, $D_t = 0.076$ m; (b) sand-air, $\rho_s = 2500$ kg/m^3, $d_p = 100$ μm, $D_t = 0.1$ m.

6. Submodels for bottom-dense region

6.1. Cluster rebound at dense bottom

Unlike the upper dilute region, the dense bottom region of a fast bed was less investigated in the past. And significant controversies appeared in the literature on the actual mechanism of

http://dx.doi.org/10.5772/68107

this region. However, it is generally agreed that two different types of axial solids holdup distributions can be found in this region, that is, the S-shaped distribution and the one exponentially decayed with height. According to Bai and Kato's systematical studies, the two different distributions would happen in a riser depending on the circulated solid flux, whether greater or smaller than the so-called "saturated carrying capacity of gas" G_s^{Bai} (in their paper noted as G_s^*) [28].

It is also agreed that fluctuations, with respect to both time and space, in the bottom dense region are very strong. Based on their measurements, Bai et al. [29] described the bottom dense region as "a more radial homogeneous cluster-dominating turbulent pattern," while Brereton and Grace [30] called it as "the cluster-like structure" indicated by its high intermittency index. Very detailed experimental investigations to the bottom region of a CFB riser were also carried out by Zhu and Zhu [31]. From their investigations, the solid concentrations at the intermittent peaks were much higher than those in free-settled clusters. Even more, in the near-wall region, the values at some plateaus reached around 0.45.

On the basis of the investigations, the authors of the paper put forward a new hypothetic model called "cluster rebound at the dense bottom" [11]. The model declares that (1) during the time that a cluster falls down and decelerates in the dense bottom, it will still absorb surrounding particles from its wake, but there will be no more particles pouring out from its nose, because of the high-flow resistance there. Thus, the solid concentration inside the cluster will increase continuously until a determinate value of $\varepsilon_{s,cl}^d$ is reached; (2) thanks to very strong mixing and interaction with the upward-moving gas-solid flow in the bottom, the much denser cluster will then be "bounced back" and leave the bottom at its original falling velocity $|u_{cl}|$ yet in the opposite direction; (3) just because of this unbalanced cluster rebound, the gas flow will gain an additional carrying capacity in this region at the basis of a uniformly saturated suspension, that is, the solid flux at type A choking G_s^*. Then, we obtain

$$G_s = G_s^* + \beta \rho_s u_{cl} (\varepsilon_{s,cl}^d - \varepsilon_{s,cl}), \tag{53}$$

where ρ_s is the particle density. From this equation, the solid concentration in rebounding clusters $\varepsilon_{s,cl}^d$ can be determined; (4) when the solid concentration in the rebounding clusters reaches its maximum value $\varepsilon_{s,cl}^{max} = 0.45$, the average value of the loosest parked beds suggested by Leva [15]; the total solid flux reaches a critical value, the saturated solid flux with once-through cluster rebound at the bed bottom

$$G_s^{rb} = G_s^* + \beta \rho_s u_{cl} (\varepsilon_{s,cl}^{max} - \varepsilon_{s,cl}); \tag{54}$$

(5) above G_s^{rb}, the gas flow will have no more ability to carry over all solid particles passing through the bottom directly. Yet, some of the particles will stay longer in this region, causing built-up of a higher dense bottom; (6) therefore, the saturated solid flux with once-through cluster rebound at the bottom G_s^{rb} can be used as a criterion to distinguish the two different distributions of axial solids holdup in the bottom region, thus it is comparable to G_s^{Bai} in Ref. [28].

6.2. Average solids holdup in dense bottom

According to the hypotheses proposed above, the modeling method for average solids holdup in the dense bottom of the bed was established as follows [11]:

1. Calculate the solid concentration in rebounding clusters $\varepsilon_{s,cl}^{d}$ and the corresponding solids holdup in the dense bottom $\varepsilon_{s,d}^{-}$, as

$$\varepsilon_{s,cl}^{d} = \varepsilon_{s,cl} + \frac{G_s - G_s^*}{\beta \rho_s u_{cl}} \tag{55}$$

$$\overline{\varepsilon}_{s,d} = \beta \varepsilon_{s,cl}^{d} + (1-\beta)\varepsilon_{s,ch}; \tag{56}$$

2. Calculate the solids holdup in the dense bottom $\varepsilon_{s,d}$, corresponding to the maximum solid concentration in rebounding clusters $\varepsilon_{s,cl}^{max} = 0.45$:

$$\varepsilon_{s,d} = \beta \varepsilon_{s,cl}^{max} + (1-\beta)\varepsilon_{s,ch}; \tag{57}$$

3. Compare the values calculated from Eqs. (56) and (57) and take the smaller one as the average solids holdup for the dense bottom;

4. At a given superficial gas velocity, repeat steps 2 and 3 with an increase of solid flux, and get the curves of $\varepsilon_{s,d}^{-}$ and $\varepsilon_{s,d}$ crossed, which determines G_s^{rb}, the saturated solid flux with once-through cluster rebound at the bottom.

The postulated behaviors of particle movement in the bottom region, that is, "once-through" or "stay longer," are also well consistent with the experimental visualizations using PEPT imaging in Ref. [32]. To distinguish the two different cases easily, we will call the case of S-shaped solids holdup distribution as a "classical" fast bed ($G_s > G_s^{rb}$), while call the case of exponentially decayed solids holdup as a "premature" fast bed ($G_s \le G_s^{rb}$). Both the classical and premature cases are "traditional" fast beds in comparison with the "high-density" fast bed characterized in Ref. [26].

Based on the above analysis, increasing solid flux G_s continuously at a constant gas velocity will lead to transitions from dilute transportation, through the premature fast bed, to the classical fast bed. Taking Bai and Kato's experiment [28] as an example, **Figure 17** gives the predicted variation of bottom solids holdup with solid flux, showing clearly these kinds of transition. The bottom solids holdup calculated by Bai and Kato's empirical correlations and the so-called "saturated carrying capacity of gas" G_s^{Bai} [28] are also given in the figure. From the figure, it is clear that the $\varepsilon_{s,d}$–G_s curves are deflected indeed near G_s^{rb} or G_s^{Bai}, but the curves are not flattened for $G_s > G_s^{rb}$ or G_s^{Bai}. The curves will be flattened at a much higher solid flux G_s^{**} with the onset of high-density fast bed, as explained before in Section 5.3. To avoid confusing this deflection with type A choking, it is better to call G_s^{rb} in its full termination "saturated solid flux with once-through cluster rebound at the bottom" or simply "saturated solid flux with cluster rebound," while calling "saturation carrying capacity" only for type A choking.

http://dx.doi.org/10.5772/68107

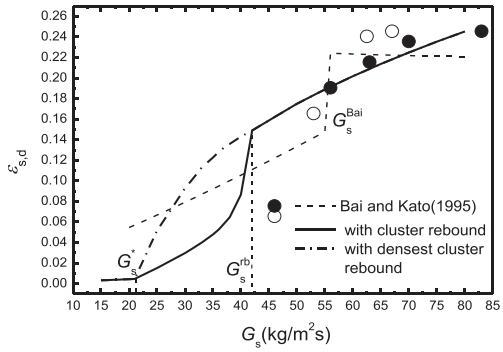

Figure 17. Predicted variation of bottom solids holdup with solid flux, and compared with Bai and Kato's experimental data and correlations [28].

6.3. Height of built-up section in dense bottom

The mechanism of how a vertical section with nearly constant solids holdup is built-up in the dense bottom has seldom been investigated. Li [33] ever tried to explain and model this process by a dynamic balance of the elutriated solid particles from the bottom region with the particles accumulated in it, which were in turn proportional to the "height of the built-up section," or simply "the dense bottom height". Using this assumption, a semi-empirical correlation between the solid flux G_s and the dense bottom height h was established [33].

The above-depicted mechanism is simple enough and looks reasonable. However, from our understanding, the solid flux to be correlated ought to be (G_s-G_s^{rb}), the extra portion beyond G_s^{rb}, but not the total one G_s. Using the data collected by Ouyang and Potter [25], the rate constant for elutriation was then reregressed [11], shown as in **Figure 18**.

$$k' = 10^{2.366}\left(\frac{\rho_g}{\rho_s - \rho_g}\right)^{1.581}\left[\frac{(u_f - v_s)^2}{d_p g}\right]^{0.471}. \tag{58}$$

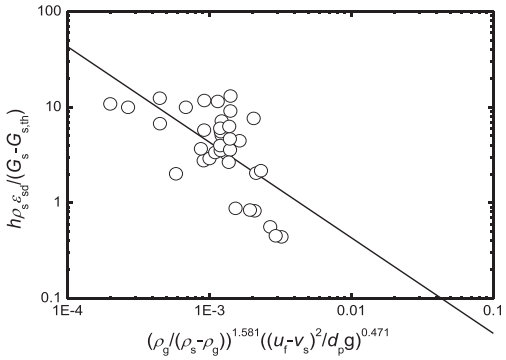

Figure 18. Multiregression result for dense bottom height h using the data collected by Ouyang and Potter [25].

And finally, the height of the built-up dense bottom can be calculated as

$$h = 10^{-2.366}\left(\frac{\rho_s - \rho_g}{\rho_g}\right)^{1.581}\left[\frac{d_p g}{(u_f - v_s)^2}\right]^{0.471} \times \frac{G_s - G_s^{rb}}{\rho_s \varepsilon_{s,d}}, \tag{59}$$

where u_f stands for the superficial gas velocity, ρ_g for gas density, while $v_s = G_s/(\rho_s \varepsilon_{s,d})$ is the nominal particle velocity in the dense bottom.

7. Axial solids holdup distribution

7.1. Momentum balance for acceleration/transition zones

In addition to the fully developed upper dilute region described in Section 4.4 and the built-up dense bottom region we have just discussed, there are also two less important zones in a classical fast bed. They are a transition zone between the two regions and an acceleration zone prior to the built-up dense section. In the acceleration zone, the particles recycled from the standpipe should be accelerated from their original downward movement to a finite upward velocity. It was assumed that in a premature fast bed, the axial solids holdup distribution decayed exponentially with height was a direct conjunction of the two zones with null built-up section in between [11].

As selecting an adequate drag coefficient is very difficult for those complicated gas-solid flows, the detailed flow mapping from commercial CFD software is usually less reliable. However, the most important principle involved in the software, that is, the momentum conservation, can still be applied when those integrated zones are considered. Compared with the solid phase, the momentum of gas and the wall friction can be neglected; the conservation of momentum between the inlet and the outlet cross sections is then written as

$$M_{out} - M_{in} = \Delta P - G, \tag{60}$$

where M_{out} and M_{in} are the solid momentum fluxes at the outlet and inlet cross sections, respectively, while ΔP stands for the pressure difference of the two sections, and G for the solid gravity per unit area within the zone.

The apparent solids holdup $\varepsilon_{s,t}^{-}$ averaged in the zone can be used to calculate the pressure difference between the lower and the upper cross sections of the acceleration/transition zones, that is, $\Delta P = h_t \rho_s g \varepsilon_{s,t}^{-}$, where h_t is the height of the zone. And the real solid concentration $\varepsilon'_{s,t}$ averaged can be used to calculate the solid gravity per unit area within the zone, that is, $G = h_t \rho_s g \varepsilon'_{s,t}$. It is supposed that $\varepsilon'_{s,t} = \eta \varepsilon_{s,t}^{-}$, where η can be considered as the contribution factor of gravity for the pressure drop. Then, we obtain

$$M_{out} - M_{in} = h_t \rho_s g(\overline{\varepsilon}_{s,t} - \varepsilon'_{s,t}) = h_t \rho_s g \overline{\varepsilon}_{s,t}(1 - \eta). \tag{61}$$

Therefore, the height of acceleration/transition zones can be calculated from the momentum flux deference between the inlet and the outlet, and the average apparent solids holdup $\varepsilon_{s,t}^{-}$ as

$$h_t = \frac{M_{out} - M_{in}}{\rho_s g \overline{\varepsilon}_{s,t}(1-\eta)}. \tag{62}$$

Putting the expressions of M_{in} and M_{out} for acceleration/transition zones, respectively, in, we have

$$h_{t1} = \frac{m_s^+ V_s^+ + m_s^- V_s^- - G_s V_d}{\rho_s g \overline{\varepsilon}_{s,t1}(1-\eta)} \text{ for transition zone,} \tag{63}$$

$$h_{t2} = \frac{G_s V_d (1+\delta)}{\rho_s g \overline{\varepsilon}_{s,t2}(1-\eta)} \text{ for acceleration zone,} \tag{64}$$

where δ stands for the coefficient of the converse momentum flux caused by the recycled solid particles moving downwards. And velocities in the equations are

$$V_s^+ = \frac{m_s^+}{\rho_s(1-\beta)\varepsilon_{s,ch}} \tag{65}$$

$$V_s^- = u_{cl} \tag{66}$$

$$V_d = v_s = G_s/(\rho_s \varepsilon_{s,d}). \tag{67}$$

Then, the equivalent momentum balance heights based on the average solids holdup of dense bottom $\varepsilon_{s,d}$ can be calculated as

$$H_{t1} = \frac{m_s^+ V_s^+ + m_s^- V_s^- - G_s V_d}{\rho_s g \varepsilon_{s,d}(1-\eta)} \text{ for transition zone,} \tag{68}$$

$$H_{t2} = \frac{G_s V_d (1+\delta)}{\rho_s g \varepsilon_{s,d}(1-\eta)} \text{ for acceleration zone.} \tag{69}$$

Adding the two equivalent momentum balance heights for the acceleration and transition zones together, we get the total momentum balance height as

$$H_t = H_{t1} + H_{t2}. \tag{70}$$

7.2. Functional description of acceleration/transition zones

As depicted in the above section, the axial solids holdup distribution exponentially decayed with height in a premature fast bed can be considered as a special case of a classical fast bed with null built-up section. Therefore, it is possible that the functional description of the acceleration/transition zones for both classical fast bed and premature fast bed can be unified to a single one. Actually, this attempt can be easily realized by the ordinate transfer from z to (z-h) for the transition zone of a classical fast bed, where h stands for the height of built-up section in the bottom. Thus, the commonly accepted exponential decay of solids holdup with bed height for the premature fast bed can be used for the unified functional description of the acceleration/transition zones as

$$\varepsilon_s = \varepsilon_{s0} e^{-\gamma z}, \tag{71}$$

where ε_{s0} stands for the solids holdup just above the air distributor of the riser, and γ for the decay constant.

Since the equivalent momentum balance heights of acceleration/transition zones have been determined above, we can simply transfer the values to the actual solids holdup distributions, in accordance with their equal impacts on the total bed pressure drop.

By some mathematical deduction, the final expressions for ε_{s0} and γ were obtained as [11]

$$\varepsilon_{s0} = \frac{\varepsilon_{s,d} - m'\varepsilon_s^*}{1 - m'} \tag{72}$$

$$\gamma = \frac{\varepsilon_{s0} - \varepsilon_{s,d}}{\varepsilon_{s,d} H_{t2}} = \frac{1}{H_{t2}} \left(\frac{\varepsilon_{s0}}{\varepsilon_{s,d}} - 1 \right), \tag{73}$$

where $m' = H_{t2}/H_t$, and ε_s^* stands for the solids holdup of the upper dilute region.

Under the same conditions of experiments in Ref. [25], the heights of transition zones were calculated with $\delta = 0$ assumed. Then, a proportionality coefficient $(1-\eta) = 0.212$ was determined from comparing those results with experimental data [25], shown as in **Figure 19**. From that, $\eta = 0.788$ was obtained, which meant that the particle gravity contributed roughly four-fifths of the total pressure drop for the zone. Now, the method to predict the axial solids holdup distribution of fast beds has been established completely.

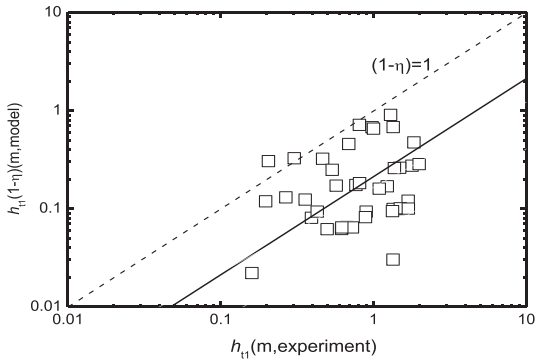

Figure 19. Comparison of the predicted heights of transition zones and the experimental data collected by Ouyang and Potter [25].

7.3. Prediction of axial solids holdup distribution

Though there were quite a lot of experimental data available in the literature, Issangya's investigation [26] for axial solids holdup distributions seemed the most systematical. FCC particles of 70 μm in diameter and 1600 kg/m^3 in density were fluidized by ambient air in a

http://dx.doi.org/10.5772/68107

riser of 0.076-m inner diameter. The operating conditions varied from dilute transportation, through the premature fast bed, the classical fast bed, until the high-density fast bed [26].

The coefficient of converse momentum flux $\delta = 2$, for the recycled particles, was applied in the calculation. As an example, **Figure 20** shows the comparisons of model predictions and the experimental data [26] for a constant gas velocity u_f= 4 m/s yet different solid fluxes of 18, 44, 68, 138, 200, and 240 kg/(m^{2}s), respectively. It can be seen from the figure that the results are somewhat reasonable.

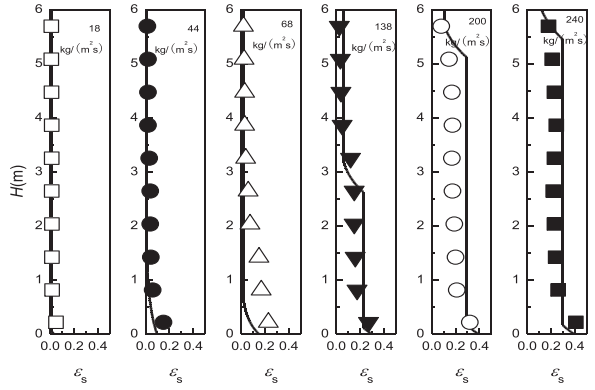

Figure 20. Axial solids holdup distributions from present model and Issangya's data, u_f= 4 m/s [26].

8. Conclusions and outlook

Based on the downward-penetrating particle flow through clusters and the analogy between a falling cluster and a rising bubble identified by the authors, a "type-A-choking-oriented separate-phase-coexistence model" for the upper dilute region of fast beds was established first. The model was then integrated with the sub-models of "cluster rebound at the dense bottom," "the momentum flux balances for acceleration and transition zones" in the lower and middle parts of the bed. The integrated model predicted successfully the axial solids holdup distributions of literature data under extremely wide operation conditions covering dilute-phase transportation, the premature fast bed, the classical fast bed, and the high-density fast bed.

To make the model system for fast fluidization have even sounder theoretical basis, more fundamental studies are expected in the future, especially those to explain further the reasons for "the four simplest integer numbers" as: "0"—in the regime of traditional fast fluidization, clusters settle down freely without outer-gas invasion; "1"—at type A choking, the terminal velocity of a particle suspension in a finite diameter riser is just equal to the terminal velocity of a single particle in an infinite fluid; "2"—at the very beginning of particle aggregation, the solid concentration in clusters is twice that in the dilute phase; "3"—the minimum solid circulating flux for fast fluidization corresponds to the type A chocking at the gas velocity of triple particle terminal velocity.

Acknowledgements

The authors would like to acknowledge the financial support from the Chinese National Natural Science Fund, Grant No. 50676062.

Author details

Ming-Chuan Zhang* and Chu Zhang

*Address all correspondence to: mczhang@sjtu.edu.cn

School of Mechanical Engineering, Shanghai Jiao Tong University, Shanghai, China

References

[1] Dry R, Beeby C J. Applications of CFB technology to gas-solid reaction. In: Grace J R, Avidan A A & Knowlton T M, editors. Circulating Fluidized Beds. London: Black Academic & Professional; 1997, Chapter 12

[2] Avidan A A. Fluid catalytic cracking. In: Grace J R, Avidan A A & Knowlton T M, editors. Circulating Fluidized Beds. London: Black Academic & Professional; 1997, Chapter 13

[3] Masten J M. Design and scale-up of CFB catalytic reactors. In: Grace J R, Avidan A A & Knowlton T M, editors. Circulating Fluidized Beds. London: Black Academic & Professional; 1997, Chapter 14

[4] Du B, Warsito W, Fan L S. Behavior of the dense phase transportation regime in a circulating fluidized bed. Industrial and Engineering Chemistry Research. 2006;**45**: 3741-3751

[5] Gidaspow D. Multiphase Flow and Fluidization: Continuum and Kinetic Theory Descriptions. Boston: Academic Press, 1994

[6] Li J, Kwauk M. Particle-Fluid Two-Phase Flow—The Energy-Minimization Multi-Scale Method. Beijing: Metallurgical Industry Press, 1994

[7] Zhu H P, Zhou Z Y, Yang R Y, Yu A B. Discrete particle simulation of particulate systems: Theoretical developments. Chemical Engineering Science, 2007;**62**:3378-3396

[8] Snider D M. An incompressible three-dimensional multiphase particle-in-cell model for dense particle flows. Journal of Computational Physics, 2001;**170**:523-549

[9] Werther J, Hartge E. Bridges between industrial practice and fundamental research in fluidization technology. In: Proceedings of CFB-11. Beijing: Chemical Industry Press; 2014. p. 1-21

[10] Zhang M C, Zhang C. A type-A-choking-oriented unified model for fast fluidization dynamics. Powder Technology, 2013;**241**:126-141

[11] Zhang M C, Zhang C. Further integration of the type-A-choking-oriented unified model for fast fluidization dynamics. Powder Technology, 2015;**286**:132-143

[12] He Y, Deen N G, ven Annaland S, Kuipers J A M. Gas-solid turbulent flow in a circulating fluidized bed riser: Experimental and numerical study of mono-disperse particle system. Industrial and Engineering Chemistry Research. 2009;**48**:8091-8097

[13] Davidson J F, Harrison D. Fluidised Particles. Cambridge: University Press, 1963

[14] Yang N, Wang W, Ge W, Wang L N, Li J H. Simulation of heterogeneous structure in a circulating fluidized bed riser by combining the two-fluid model with the EMMS approach. Industrial and Engineering Chemistry Research. 2004;**43**:5548-5561

[15] Leva M. Fluidization. New York: McGraw-Hill Book Company, 1959

[16] Yang W C. A mathematical definition of choking phenomenon and a mathematical model for predicting choking velocity and choking volume fraction. AIChE Journal. 1975;**21**:1013-1015

[17] Yang W C. Criteria for choking in vertical pneumatic conveying lines. Powder Technology, 1983;**35**:143-150

[18] Yang W C. Estimating the solid particle velocity in vertical pneumatic conveying lines. Industrial and Engineering Chemistry Fundamentals. 1973;**12**:349-352

[19] Yang W C. Correlations for solid friction factors in vertical and horizontal pneumatic conveyings. AIChE Journal. 1974;**20**:605-507

[20] Xu G, Nomura K, Gao S, Kato K. More fundamentals of dilute suspension collapse and choking for vertical conveying systems. AIChE Journal. 2001;**47**:2177-2196

[21] Bi H T, Grace J R, Zhu J X. On types of choking in vertical pneumatic systems. International Journal of Multiphase Flow, 1993;**19**:1077-1092

[22] Richardson J F, Zaki W N. Sedimentation and fluidization: Part I. Trans. Inst. Chem. Transport Bed. Chemical Engineering Science. 1954;**40**:259-267

[23] Harris A T, Davidson J F, Thorpe R B. The prediction of particle cluster properties in the near wall region of a vertical riser. Powder Technology, 2002;**127**:128-143

[24] Yousfi Y, Gau G. Aerodynamique de l'ecoulement vertical de suspensions concentrees gaz-solides-I: regimes d'ecoulement et stablilite aerodynamique. Chemical Engineering Science, 1974;**29**:1939-1946

[25] Ouyang S, Potter O E. Consistency of circulating fluidized bed experimental data. Industrial and Engineering Chemistry Research. 1993;**32**:1041-1045

[26] Issangya A S, Bai D, Bi H T, Lim K S, Zhu J, Grace J R. Suspension densities in a high-density circulating fluidized bed riser. Chemical Engineering Science. 1999;**54**:5451-5460

[27] Grace J R, Issangya A S, Bai D, Bi H, Zhu J. Situating the high-density circulating fluidized bed. AIChE Journal. 1999;**45**:2108-2116

[28] Bai D, Kato K. Quantitative estimation of solids holdups at dense and dilute regions of circulating fluidized beds. Powder Technology, 1999;**101**:183-190

[29] Bai D, Shibuya E, Masuda Y, Nakawaga N, Kato K. Flow structure in a fast fluidized bed. Chemical Engineering Science, 1996;**51**:957-966

[30] Brereton C M H, Grace J R. Microstructure aspects of the behavior of circulating fluidized beds. Chemical Engineering Science, 1993;**48**:3565-2572

[31] Zhu H, Zhu J. Characterization of fluidization behavior in the bottom region of CFB risers. Chemical Engineering Journal, 2008;**141**:169-179

[32] Chen C W, Seville J, Yang Z, Baeyens J. Particle motion in the CFB riser with special emphasis on PEPT-imaging of the bottom section. Powder Technology, 2009;**196**:318-325

[33] Li Y C. Introduction of Fluidization Process Engineering (in Chinese). Beijing: Science Press; 2008